GEOPHYSICS, VOL. 77, NO. 1 (JANUARY-FEBRUARY 2012); P. E57–E65, 7 FIGS.
10.1190/GEO2011-0081.1

Seismically regularized controlled-source electromagnetic inversion

Vanessa Brown[1], Kerry Key[2], and Satish Singh[3]

ABSTRACT

Marine controlled-source electromagnetic (CSEM) data can be highly sensitive to the presence of resistive hydrocarbon bearing layers in the subsurface. Yet, due to the relatively poor depth resolution of CSEM data and the smoothness constraints imposed by electromagnetic (EM) inversion methods, the resulting resistivity models are often highly smoothed-out, typically underestimating the reservoir resistivity and overestimating its thickness. Conversely, seismic full-waveform inversion (FWI) can accurately recover the depths of seismic velocity changes, yet, is relatively insensitive the presence of hydrocarbons. In spite of their low depth resolution, CSEM data have been shown to be highly sensitive to the resistivity-thickness product of buried resistive layers, suggesting that if the thickness of a target layer can be constrained a priori, very accurate resistivity estimates may be obtained. We developed a method for leveraging the high depth resolution of FWI into a standard CSEM inversion algorithm so that the resulting resistivity models have depth constraints imposed by the seismic structure and consequently may obtain more accurate resistivity estimates. The seismically regularized CSEM inversion that we propose is conceptually similar to minimum-gradient support (MGS) regularization, but it uses regularization weights based on gradients in the seismic velocity model rather than the self-reinforcing model resistivity gradients used in the typical MGS scheme. A suite of synthetic model tests showed how this approach compares with standard smooth and MGS inversions for a range of rock types and hence, levels of correlation between the seismic and resistivity structures, showing that a significantly improved resistivity model can be obtained when the velocity and resistivity profiles are correlated in depth. We also found that this regularization weighting method can be extended to use depth constraints from geophysical data other than seismic velocity models. Tests on a real data example from the Pluto gas field demonstrated how the regularization weights can also be set using a nearby well log, resulting in a more compact estimate of the reservoir resistivity than possible with a standard smooth inversion.

INTRODUCTION

Over the past decade, the marine controlled-source electromagnetic (CSEM) method has been adopted and commercialized for offshore hydrocarbon exploration (e.g., Eidesmo et al., 2002; Constable, 2010). The utility of the CSEM method resides in its sensitivity to resistive hydrocarbon fluids in place of saline pore fluids, in which the corresponding electrical resistivity can span several orders of magnitude, from conductive brines and seawater to highly resistive reservoirs. Although this makes CSEM attractive to the exploration geophysicist, it also leads to large variations in the measured electromagnetic fields, contributing further to an already ill-posed and nonunique problem. For these reasons, the inverse problem generally can not be solved using local perturbation methods; instead, regularization must be introduced to stabilize the inverse solution.

Regularization involves the introduction of an additional term or set of terms into the inverse problem that serves to steer the inversion away from extreme models or model variations. A classic example is the roughness penalty applied by Occam's inversion (Constable et al., 1987), in which a norm on the gradient of model parameters forces the solution toward smooth models that contain the minimum amount of structure required to fit a given data set. More recent approaches have considered regularization operators that penalize the support of the model parameters or their gradient (e.g., Portniaguine and Zhdanov, 1999), producing models with

Manuscript received by the Editor 1 March 2011; revised manuscript received 15 June 2011; published online 8 February 2012.
[1]Scripps Institution of Oceanography, University of California, San Diego, California, USA; Institut de Physique du Globe de Paris, Paris, France. E-mail: brown@ipgp.fr.
[2]Scripps Institution of Oceanography, University of California, San Diego, California, USA. E-mail: kkey@ucsd.edu.
[3]Institut de Physique du Globe de Paris, Paris, France. E-mail: singh@ipgp.fr.

more focused and sharply varying features than possible with traditional smooth inversion.

Despite these innovations, electromagnetic (EM) data still suffers from a relatively low depth resolution. Although the frequency range of EM data allows for an intrinsic depth resolution that is not possible with static potential field measurements such as gravity and magnetics, the depth resolution using EM methods is relatively poor compared to that of many seismic methods. However, the CSEM method has been shown to be highly sensitive to the resistivity-thickness product of buried resistive layers (e.g., Constable and Weiss, 2006), allowing modeling techniques that fix the layer thickness a priori to obtain very accurate resistivity estimates (e.g., Key, 2009). Furthermore, the ability to distinguish resistive hydrocarbons from conductive brines makes the EM method an important tool for offshore exploration.

The situation has led to methods that take advantage of the respective strengths of both seismic and EM data such that an improved interpretation can be made over that from either method alone. The most common methods in use are joint inversions, in which both seismic and EM data are simultaneously inverted. This can be done through physical property models that link electrical conductivity to seismic velocity, but it is more commonly accomplished through cross-gradient regularization (e.g., Gallardo and Meju, 2003). In the cross-gradient technique, regularization terms are introduced to penalize misaligned gradients in the seismic and EM models, thereby steering the velocity and resistivity inversions toward structural similarity.

Although the cross-gradient approach has proven effective, questions remain about how to balance the dramatically different resolutions for each data type. Consider the case in which one data set has significantly higher spatial resolution than the other, such that the lower resolution data set does nothing to change the joint-inversion result of the higher resolution data set. Although the inverted model from the lower resolution data may benefit from the joint-inversion, it is not clear that the full complexity of the joint-inversion is required to achieve the same end result.

Here, we consider an alternative approach to joint inversion that could be labeled *guided* inversion. We ask the question of how to effectively incorporate high-resolution seismic velocity models into an EM inversion, such that some of the lower depth resolution of the EM data can be overcome with the seismic constraints. To do this, we examine the form of the regularization operators commonly used for EM inversion and find that we can simply multiply the standard smooth inversion regularization by weighting terms based on the gradient of the velocity model such that structural similarities are encouraged in the resistivity model. Therefore, the method we propose will work best when the boundaries of resistivity and velocity changes occur at similar depths. Because correlated properties will not always be the case when dealing with the complexity of real-world problems, we perform a suite of empirical tests to examine how the method performs when the properties are correlated, uncorrelated, and when the seismic model is either incorrect or has significantly different character than the resistivity model. The seismic regularization method we present below is an easy to implement tool that can be used to augment and complement the suite of existing inversion methods applied for CSEM interpretation.

SEISMIC REGULARIZATION

We introduce the seismic regularization concept by showing its application in a standard EM inversion algorithm (Occam's inversion, Constable et al., 1987); however, we note that seismic regularization is general and could be applied to other regularized inversion techniques used for EM geophysics. Occam's inversion seeks to minimize the following unconstrained regularized functional

$$U_{\text{occ}} = \mu^{-1}[\|\mathbf{W}_d(\mathbf{d} - F(\mathbf{m}))\|^2 - \chi_*^2] + R(\mathbf{m}), \qquad (1)$$

where $\mathbf{d}$ represents the data vector, $F(\mathbf{m})$ is the forward response of the parameterized conductivity model $\mathbf{m}$, $\mathbf{W}_d$ is a diagonal matrix of inverse data errors and χ_*^2 is the target misfit. The Lagrange multiplier μ serves as a trade-off parameter that balances the goodness-of-fit term in brackets with the regularization term R. Because EM inversion is ill-posed, the regularization term R is included to stabilize the inverse problem by protecting against overfitting the data, which tends to produce highly oscillatory models. Although regularized inversion has strong theoretical underpinnings (e.g., Tikhonov and Arsenin, 1977), the specific form of the regularization operator is highly flexible, and R is typically some measure of the model size or its variations. Occam's inversion searches for the smoothest model fitting the data by regularizing against the model roughness

$$R_{\text{occ}}(\mathbf{m}) = \|\mathbf{W}_{\text{occ}}\partial\mathbf{m}\|^2, \qquad (2)$$

where ∂ is a differencing operator applied to the model elements and $\mathbf{W}_{\text{occ}}$ is a diagonal weighting matrix; ∂ is typically set to approximate the gradient or first difference in adjacent model parameters, and $\mathbf{W}_{\text{occ}}$ is usually the identity matrix, so that the regularization is applied uniformly throughout the model domain. However, when the model structure has known boundaries, the smoothness constraint can be relaxed at these boundaries by specifying small or zero weights in the corresponding diagonal elements of $\mathbf{W}_{\text{occ}}$. This is usually done in a somewhat ad hoc manner, for example, by an interpreter who visually selects the appropriate depths from a seismic model. The weights can also be adjusted to bias the inversion toward heavier regularization at certain regions of the model. For example, because EM resolution tends to decrease with depth, the elements of $\mathbf{W}_{\text{occ}}$ can be set to increase with depth and thereby enforce a smoother model with depth.

The introduction of the model roughness regularization R_{occ} in Occam's inversion represented a significant milestone in the development of EM modeling techniques because it provided a tool for obtaining reasonable inversion models, whereas previous unregularized inversions were prone to spurious and wildly oscillating models of questionable reliability (Constable et al., 1987). However, there are many cases where the smooth inversion models produced by this regularization are unsatisfactory, particularly when the geologic structure is expected to vary sharply. In part, smooth inversion models reflect the degree of nonuniqueness in an EM data set in which the inversion has been biased toward finding a smooth model that fits the data. More recent efforts have focused on regularization operators that instead bias the inversion toward models with sharply varying contrasts in structure while still maintaining the stabilizing effects of regularization. A popular variation is the minimum-gradient support (MGS) functional (Portniaguine and Zhdanov, 1999)

$$R_{\text{mgs}}(\mathbf{m}) = \left\| \frac{\partial \mathbf{m}}{(\partial \mathbf{m}^2 + \beta^2)^{1/2}} \right\|^2 = \|\mathbf{W}_{\text{mgs}} \partial \mathbf{m}\|^2. \quad (3)$$

The R_{mgs} regularization penalizes against the depth interval or area over which a gradient in the model parameters occurs. The parameter β serves as a knob for specifying the minimum-gradient cutoff level and ensures a nonzero denominator. Inversion using R_{mgs} tends to produce sharp gradients in model structure between layers of constant properties. Although this is often pleasing from a geologic interpretation point of view, it is still subject to the nonuniqueness inherent in EM inversion. As we demonstrate in the next section, models produced using R_{mgs} can suffer from inaccurate interface depths and layer thicknesses. Because CSEM inversion is predominantly sensitive to the resistivity-thickness product of a resistive layer (e.g., Constable and Weiss, 2006), this depth inaccuracy also produces inaccurate resistivities, thereby limiting the potential for quantitative interpretation of the inverted resistivity model.

Comparison of the right-hand sides of equations 2 and 3 shows that R_{mgs} and R_{occ} only differ in the form of the weighting matrix; it is therefore straightforward to modify an existing inversion algorithm to accommodate both approaches. This simplicity has led us to suggest a novel method for including seismic constraints during EM inversion. We simply propose a weighting function that is based on the gradient in seismic velocity, rather than electrical conductivity. Specifically, we define the seismically weighted regularization operator:

$$R_{\text{smgs}}(\mathbf{m}) = \left\| \frac{\beta \partial \mathbf{m}}{(\tilde{\partial}\mathbf{v}^2 + \beta^2)^{1/2}} \right\|^2 = \|\mathbf{W}_{\text{smgs}} \partial \mathbf{m}\|^2, \quad (4)$$

where $0 < \mathbf{W}_{\text{smgs}} < 1$, $\mathbf{v}$ is a seismic parameter (i.e., P- or S-velocity), and $\tilde{\partial}\mathbf{v}$ is the mean gradient in velocity over a small window. In the examples shown here, we use a 60-m window centered at the depth of interest to minimize the source signature in the seismic profile and to minimize the effects of small-scale velocity gradients associated with noise in the inversion. The 60-m window is approximately $\lambda/2$, where λ is the highest frequency source wavelength.

Although R_{smgs} is similar to the minimum-gradient support (MGS) regularization R_{mgs}, the weights are derived from a seismic velocity model. Therefore, R_{smgs} should produce resistivity models with sharp contrasts like those obtained with MGS regularization, but the depths from R_{smgs} will be biased to be coincident with the depths of large gradients in the seismic model. In this way, structural similarities are encouraged in the EM inversion. Because seismic models typically have much higher depth resolution than possible with EM methods, R_{smgs} should produce more accurate layer depths than R_{mgs}, which in turn should lead to more accurate resistivities. An implicit assumption in the operator R_{smgs} is that the large-scale seismic and resistivity structural boundaries are correlated in depth. If this is not the case, then there is likely to be little benefit from using R_{smgs} over R_{occ}. However, when resistivity and velocity are expected to be correlated, R_{smgs} is a simple deterministic method that can be used to incorporate seismic depth constraints in EM inversion, without requiring the theoretical or numerical complexities of a true joint-inversion method.

Here, we show how the regularization operator is specifically incorporated in Occam's inversion. Equation 1 is minimized after linearization about a model $\mathbf{m}_i$, giving the iterative update for next model in the sequence $i = 1, 2, \ldots N$ as

$$\mathbf{m}_{i+1} = [\mu(\mathbf{W}^T\mathbf{W}\partial^T\partial) + (\mathbf{W}_d\mathbf{J}_i)^T\mathbf{W}_d\mathbf{J}_i]^{-1}[(\mathbf{W}_d\mathbf{J}_i)^T\mathbf{W}_d\hat{\mathbf{d}}], \quad (5)$$

where the modified data vector $\hat{\mathbf{d}}$ is

$$\hat{\mathbf{d}} = \mathbf{d} - F(\mathbf{m}_i) + \mathbf{J}_i\mathbf{m}_i, \quad (6)$$

and $\mathbf{J}_i$ is the Jacobian matrix for the ith model.

Equation 5 is equivalent to the original Occam formulation, but here it contains the regularization weighting matrix $\mathbf{W}$, which should be set to the form appropriate to the specific regularizations described above. Equation 5 is solved repeatedly until the current model meets the specified χ^2_* value, after which subsequent iterations are used to search for a model at the target misfit but with the lowest roughness measure R (i.e., the smoothest model). Other details of Occam's inversion, including its unique method for selecting the Lagrange multiplier μ, are discussed in Constable et al. (1987).

Seismic full-waveform inversion

Before presenting examples that demonstrate the performance of seismic regularization, we first discuss our method of choice for obtaining high-fidelity seismic velocity models. Seismic full-waveform inversion (FWI) is advantageous over ray-tracing or tomographic methods because it uses the full information content of a seismic signal during the inversion; it therefore offers great potential for recovering detailed models of subsurface elastic properties, and such models will be useful for the seismic regularization approach. FWI starts with an initial low-resolution velocity model that has been obtained during a preprocessing step, such as NMO and time travel analysis as described in (Shipp and Singh, 2002). FWI is then used to find a final high-resolution velocity model that fits the short to long offset seismic waveforms. The FWI scheme used here utilizes a time-domain approach to propagate the elastic wavefield through a finite difference grid of parametrized elastic properties (Shipp and Singh, 2002). Starting with the initial elastic properties model $\mathbf{v}_i$, the residual S is calculated by taking sample by sample differences between the observed and predicted data sets. The iterative model updates of the FWI are computed using a gradient method that minimize S. These are found by updating the model parameters in the opposite direction of the gradient of S according to

$$\mathbf{v}_{i+1} = \mathbf{v}_i - l\nabla S, \quad (7)$$

where ∇S is the gradient of residual, l is some calculated step length. Following the inversion scheme of Tarantola (1986), the residual gradient is computed using the crosscorrelatation between the forward propagated and backward propagated residual wavefield, thereby avoiding explicit computation of the Jacobian. This residual gradient is used as the descent direction and is buffered against nonlinearities through the step length l. A full derivation is given in Tarantola (1986). To avoid slipping into local minima, the inversion is decomposed by scale, by which only low-frequency (and/or long offset) data are initially inverted to constrain the larger

features, whereas successively higher frequencies (and/or short offsets) are added to refine smaller features of the model (Virieux and Operto, 2009). Using long-offset data combined with the multiscale approach, the FWI method can recover the intermediate wavelengths. The resolution in the full-waveform inversion scheme is $\lambda/4$ (Neves and Singh, 1996; Shipp et al., 2005), where λ is the source wavelength from the highest frequency. On the other end, the method of full-waveform inversion requires that the features in the starting model must be within $\lambda/4$ in wave propagation when using the lowest frequency available for inversion or else there is a risk that the inversion could slip into an incorrect local minima. To converge from a starting model to the correct model, low frequencies and/or an accurate starting model is required. Although the FWI scheme solves for both P- and S-wave velocities, here, we concentrate on only the P-wave velocity results.

SYNTHETIC EXAMPLES

In this section, we demonstrate the performance of seismic regularization with synthetic model studies that are illustrative of offshore hydrocarbon exploration problems. Although we have tried to maintain generality in our approach, our initial tests are restricted to 1D models. Synthetic CSEM data were generated using the open-source frequency-domain CSEM code Dipole1D (Key, 2009). Inline CSEM responses to 20-km source-receiver offset were computed for a suite of frequencies (0.1, 0.3, 0.5, 0.7, 1.3 Hz) corresponding to the strong harmonics of a modern broadband transmitter waveform (Myer et al., 2011). To mimic real data with various sources of relative and absolute uncertainty, 5% Gaussian noise was added and data below a typical system noise floor of 10^{-15} V/Am^2 were removed. All CSEM inversions were fit to a root-mean-squared (rms) misfit of 1.0 and the β parameter in the R_{mgs} and R_{smgs} regularizations was set in the range of 0.01–1, depending on the mean gradients in the final velocity model. The CSEM inversions all used a 1-ohm-m half-space as the starting model. Synthetic seismic data at frequencies from 6 to 36 Hz and source-receiver offsets up to 10 km were generated with the forward modeling code of Shipp and Singh (2002). The FWIs used a P-wave velocity starting model that is identical to the true model but without the target layers that are described below. The seismic and resistivity models we test are derived from a background sediment compaction model (Bahr et al., 2001) that was adjusted for differences in rock and fluid properties. Depending on the fluid and matrix types, Archie's Law, the Gassman equations, and modified Hashin-Shtrikman bounds were used to assign the electrical resistivity and seismic P-wave velocity, respectively (e.g., Carcione et al., 2007). All models used a 1-km ocean depth.

Step Model

The first synthetic study focuses on a brine saturated sedimentary model that includes a step decrease in porosity associated with a lithology change at 2-km depth below the sea surface. Figure 1 shows the true seismic model, the corresponding FWI, the true resistivity model and the CSEM inversions computed using the R_{occ}, R_{mgs}, and R_{smgs} regularizations. The FWI started from a smooth model and found the large step velocity increase to within 25-m depth of the true model. Both the location and size of the velocity jump are well recovered with the FWI. As expected, the standard smooth inversion R_{occ} was unable to recover the sharp jump in resistivity; instead it has a smooth resistivity increase that extends over 800-m depth range. The MGS regularization R_{mgs} does better at recovering the discrete jump in resistivity, but the depth is in error by about 100 m. Conversely, the seismically regularized CSEM inversion R_{smgs} is able to find the depth of the jump to less than 25-m error. This is expected because the seismic model was used to form the regularization weights $\mathbf{W}_{smgs}$. Figure 1b shows that $\mathbf{W}_{smgs}$ is generally uniform throughout the depth range but contains a sharp decrease around the location of the step, hence the penalty for resistivity variations at this depth is much less than the penalty at other depths. This simple example demonstrates how a seismic velocity model can be effectively used to bias the CSEM inversion through seismic regularization. In the next section we consider some more difficult targets.

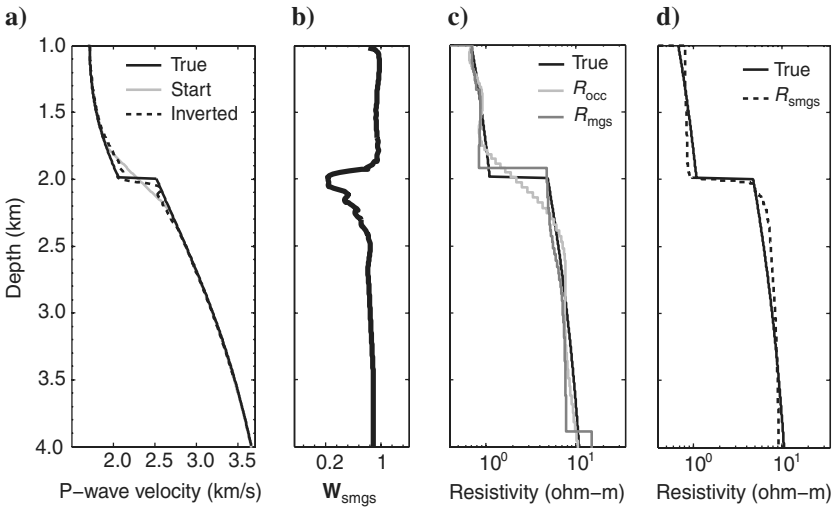

Figure 1. Step model example: (a) The true P-velocity model, the starting model, and full-waveform inversion result; (b) the weighting function $\mathbf{W}_{smgs}$; (c) the true resistivity model with inversion results from the standard Occam regularization R_{occ} and the MGS regularization R_{mgs}; and (d) the seismically regularized R_{smgs} inversion.

Hydrocarbon Prospects

Now, we examine how seismic regularization performs for a few hydrocarbon prospect models. Figure 2 shows the four scenarios under consideration. The models include a compacted sedimentary background with a suspected target layer that is 1 km below the seafloor and 100 m thick. Model A has a target consisting of a sandstone reservoir saturated with oil. Model B is the same as model A, but instead has a brine-filled reservoir. The target layer in model C has a high gas saturation, whereas in model D, the target has a low gas saturation. The corresponding velocity and resistivity models are shown in Figure 5. This suite of models contains various combinations of high- or low-velocity anomalies and either an increase or none in resistivity, providing a simple test bed for accessing the performance of R_{smgs} when structures are correlated or uncorrelated. An example of the FWI synthetic

seismic data and fit is shown in Figure 3 for model A. Figure 4 shows the level of CSEM responses generated by model A by the introduction of a reservoir, as well as examples of the synthetic data and model response fitting to rms 1.0. Inversion models obtained from the FWI and CSEM inversions are shown in Figure 5.

Models A and B

Models A and B have the same seismic profile despite the lack of hydrocarbons in model B, representing an exploration scenario where the seismic interpretation may be ambiguous due to a similar velocity from oil or brine in the target layer. The FWI reliably recovers the layer depth and sharp velocity increase for both models. The true resistivity increases to 45 ohm-m in the target layer for model A due to the oil saturation, whereas model B does not contain an increase because its target layer is only filled with brine. The R_{occ} and R_{mgs} inversions both indicate that a resistive layer is present for model A, but the size of the resistive layer is poorly recovered. However, in both cases, the resistivity-thickness product of the layer is close to that of the true model. Although the smooth inversion R_{occ} does a good job recovering the monotonic increase in resistivity with depth for the background sediments, the MGS inversion R_{mgs} poorly approximates this trend, and instead, has a large step increase in resistivity at about 3.5 km depth. Conversely, the seismically regularized inversion R_{smgs} accurately recovers the depth and resistivity of the target layer, as well as the monotonic increase in resistivity with depth. The relative error for the reservoir resistivity is only 5%–10% for R_{smgs}, whereas R_{mgs} underestimates the resistivity by about 80%. For the null-hypothesis represented by model B, all three CSEM regularizations produce models with little structure in the vicinity of the target layer, with the smooth inversion R_{occ} best recovering the monotonic increase in background resistivity. The seismically regularized inversion R_{smgs} contains a small step at the target layer due to the small value of the weights in $\mathbf{W}_{smgs}$ at the target layer's boundaries (note that inversions for models A and B used identical seismically derived weights $\mathbf{W}_{smgs}$). However, together the seismic constrained and the smooth inversion results confirm that despite the seismically inferred target layer, it is unlikely to be filled with resistive hydrocarbons.

Taken together, the R_{occ}, R_{mgs}, and R_{smgs} inversions all indicate the presence of a significant resistive layer for model A, but at most, only a very small resistivity change for model B.

Model C

Model C contains a small decrease in P-wave velocity in the target layer due to the presence of gas. The seismic FWI accurately recovers the layer depth and small velocity change. The true resistivity of the target layer for this model increases to around

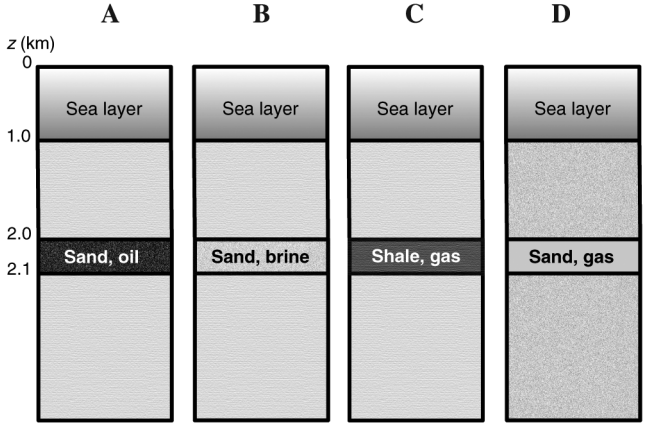

Figure 2. Models A–D used in synthetic studies.

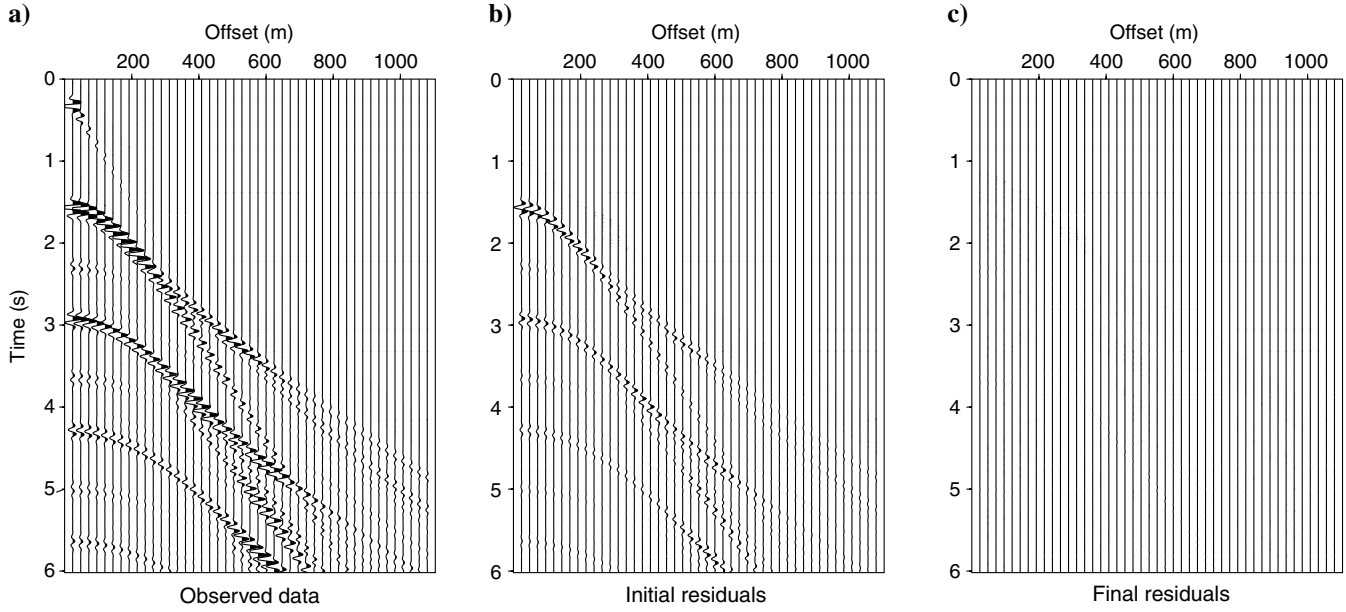

Figure 3. Synthetic seismic data plots and FWI residuals for model A example: (a) the synthetic observed data generated, (b) the initial residuals using a starting model with no reservoir layer, (c) the final residuals after multistage full-waveform inversion and the target reservoir layer is recovered.

30 ohm-m due to the gas saturation. Both the R_{occ} and R_{mgs} CSEM inversions recover the resistivity increase around the layer, but similar to the inversions for model A, they underestimate the resistivity and overestimate the thickness (yet conserve the resistivity-thickness product for the layer.) The smooth inversion R_{occ} places the peak resistivity near the correct depth, whereas the R_{mgs} inversion has the layer significantly shallower than the true model. Despite only a small change in velocity at the layer boundaries, the seismically regularized inversion identifies the depth of the reservoir well. It is not as sharp as model A due to the smaller velocity contrasts and smaller resistor. Again, the monotonic background trend of the model is well capture by the R_{smgs} inversion, although there are small wiggles in the shallow resistivity that are not present in R_{smgs} inversions for model A and model B.

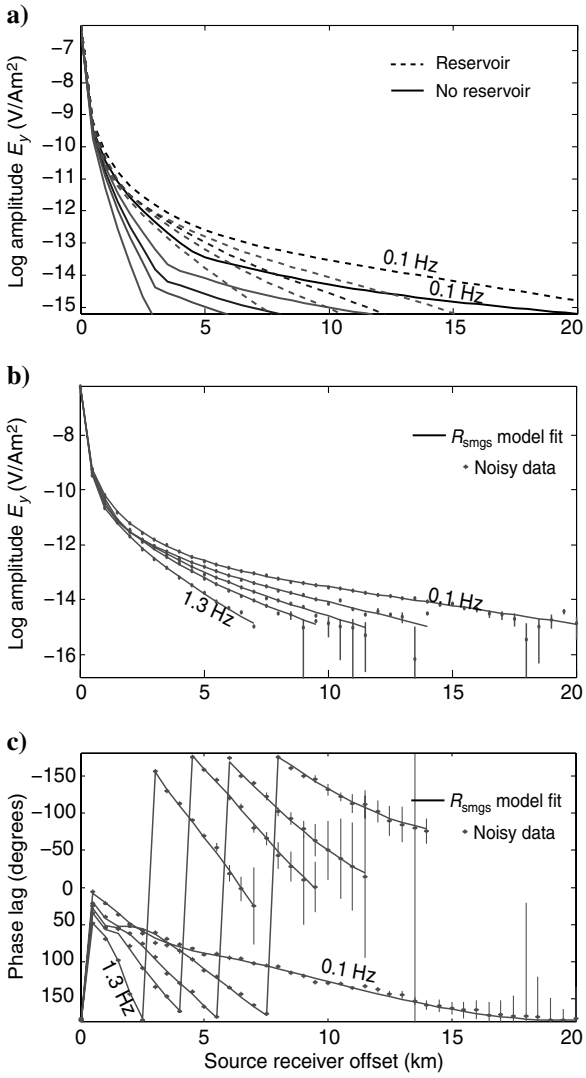

Figure 4. Synthetic CSEM data for model A: (a) CSEM response for model A with no target reservoir (solid lines) and with a target reservoir (dashed lines) shown for five frequencies (0.1, 0.3, 0.5, 0.7, and 1.3 Hz), (b) the synthetic noisy amplitude, and (c) phase responses and the model response fitting to rms 1.0 when using the seismically weighted regularization approach.

Model D

Model D contains a larger decrease in P-wave velocity in the target layer due to a gas sand. Because the saturation is lower than model C, the resistivity only increases to about 8 ohm-m (about a factor of two-to-three more than the background at this depth). Again, the seismic FWI accurately recovers the layer depth and velocity change. However, for this model, neither the R_{occ} nor R_{mgs} CSEM inversions are able to recover the relatively small increase in resistivity in the target layer, although both have background resistivities that are slightly larger than the true background. The seismically regularized inversion R_{smgs} has a small increase in resistivity that begins at the base of the target layer, but overall is unable to positively identify the presence of the moderately resistive gas layer.

Effect of inaccurate depths and uncorrelated structures

As the previous examples demonstrate, the seismic regularization technique performed the best when both the seismic and EM models have large contrasts that are correlated in depth. Now, we examine what happens when the seismic and EM structures are uncorrelated by moving the seismic structure for model A by 100–500 m in depth while keeping the EM resistor at the same depth (2000–2100 m). The resulting inversion models are shown in Figure 6. When the seismic layer has its depth moved 100 m shallower, the CSEM inversion can still reach an rms misfit of 1.0 and has a sharp resistive layer within the depth of the perturbed seismic layer, illustrating that small depth errors in the seismic inversion will have little impact on the CSEM inversion. When the seismic layer is moved 200 m deeper, the CSEM inversion does poorer at recovering the reservoir, but still contains a distinct peak at the (incorrect) seismic layer depths. When the seismic layer is moved 550 m shallower, the CSEM inversion no longer places a resistor within the depth range of the seismic layer; instead a smooth resistive layer is placed deeper just above the true resistive layer depths, and this is compensated by an obviously incorrect very-low-resistivity layer at the depth of the seismic layer. In this case, the presence of the deeper resistor in the CSEM inversion indicates that the seismic and resistivity structures are uncorrelated, and therefore, that the seismic regularization approach is not applicable for improving the CSEM inversion. We can conclude that the CSEM inversions have depth resolution on the order of 100–200 m, and therefore, that the seismic regularization approach will work well for correlated resistivity and velocity structures when the seismic depths are accurate to within 100–200 m, although this will certainly vary with the target depth because CSEM resolution rapidly decreases with depth.

Our example model studies have only considered large-scale model features. Due to the diffusive nature of low-frequency EM fields, the resolution of fine-scale layering at depth is not possible with CSEM data because they contain little sensitivity to such features. Therefore, we expect there will be no benefit from using the seismic regularization technique for resolving the fine-scale layering. For the large-scale features considered in our examples, we see that the seismic regularization can significantly improve the CSEM estimate of the target resistivity. Even in the case in which the seismic layer is 100 m too shallow, the seismically regularized CSEM inversion still recovers an accurate target resistivity, and hence, could be used for quantify reservoir saturation.

EXTENSION TO WELL LOGS WITH A REAL DATA EXAMPLE

Although we have so far focused on regularization weighting using seismic velocity models, the regularization weighting approach developed here can easily be adapted to other physical property measurements that are a priori assumed to be correlated with the CSEM derived resistivity. For example, the regularization weights could be formed using the highly detailed resistivity profiles obtained from nearby well logs, rather than seismic velocities. In this case, the regularization term is biased by weights formed from the well-log gradient:

$$R_{\text{well}}(\mathbf{m}) = \left\| \frac{\partial \mathbf{m}}{(\partial \mathbf{m}_{\text{well}}^2 + \beta^2)^{1/2}} \right\|^2 = \|\mathbf{W}_{\text{wmgs}} \partial \mathbf{m}\|^2. \quad (8)$$

We demonstrate the effectiveness of this regularization using a well log and CSEM data obtained at the Pluto gas field offshore the northwest coast of Australia. The data and well log were previously described in Key and Lockwood (2010). Figure 7 shows the well log and the inversion results from using each of the three regularizations, all fitting the data to an rms misfit of 1.0. The smooth inversion gives an indication of a resistivity increase around the

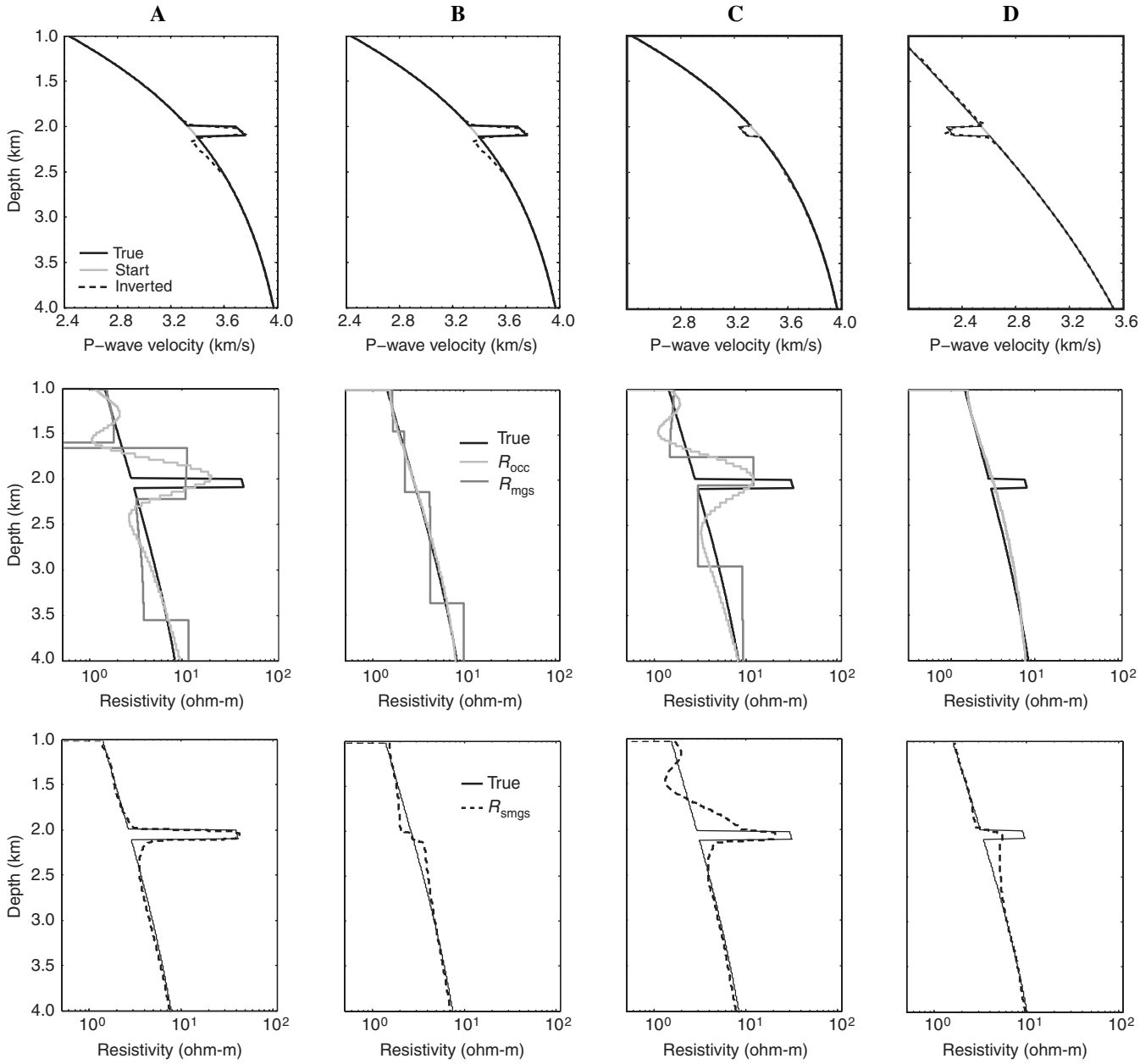

Figure 5. Seismic full-waveform inversions and CSEM inversions for models A, B, C, and D from Figure 2. The top row shows the seismic full-waveform inversions. The middle row shows CSEM inversion results for the standard smooth regularization R_{occ} and minimum gradient support regularization R_{mgs}. The bottom row shows CSEM inversion results for the seismically weighted regularization R_{smgs}.

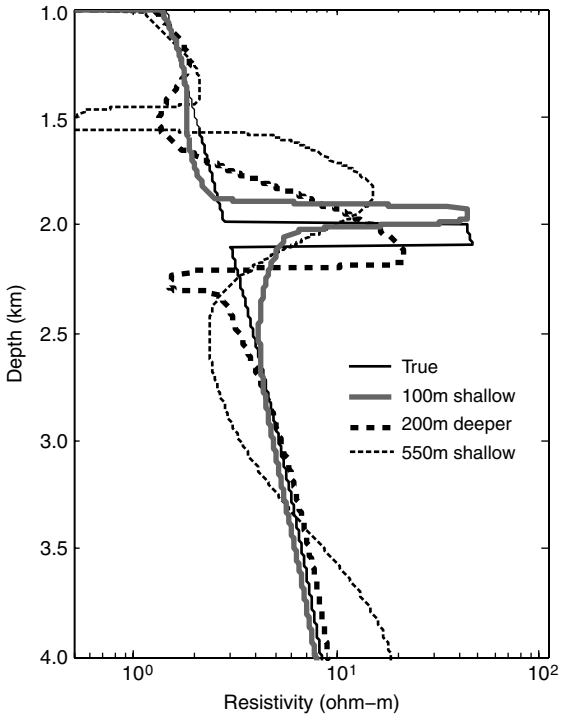

Figure 6. Example of seismic regularized CSEM inversion results from using incorrect seismic models where the high-velocity layer is perturbed by 100, 200, and 550 m from the truth.

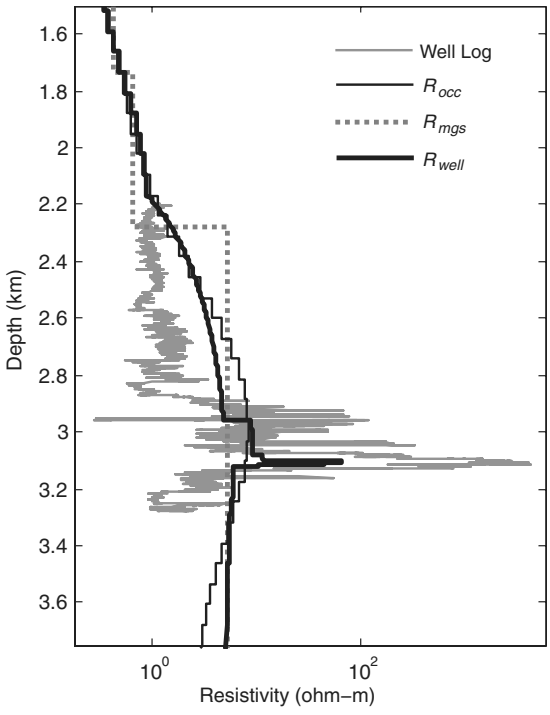

Figure 7. Example of regularization weighting using a nearby well log. The well log, the smooth inversion, the MGS inversion, and the well-log regularized inversion are indicated in the legend.

reservoir depth at about 3 km, but it is too broad to be quantitatively useful or indicative of a gas field. The R_{mgs} inversion has a simple step increase at 2.3-km depth that offers little indication of a gas field. In both of these cases, the inversion has smeared out the thin resistive gas field over a much broader depth interval than is suggested by the discrete structure in the well log. Conversely, the well-log regularized inversion R_{well} places a thin resistive layer at the depth where the well log indicates high resistivity values.

CONCLUSIONS

We have developed a simple method for incorporating seismic constraints into EM inversion through the use of special regularization weights. This seismic regularization method is conceptually similar to MGS regularization in that it produces blocky or sharply focused models. However, unlike the MGS method, it does not suffer from the resistivity-thickness product ambiguity because the structural boundary depths are constrained by the seismic full-waveform inversion model. This approach provides a formal method for the inclusion of seismic structure into EM inversion but avoids the complexities of true joint-inversion methods.

Test examples show that where resistivity and velocity variations are coincident, the seismically regularized CSEM inversions can more accurately recover the resistivity of hydrocarbon layers than standard smooth regularization or MGS regularization. This approach can be used to reduce seismic ambiguity, where a target structure identified in the seismic model can be tested for a resistivity anomaly with CSEM inversion. The ability to more accurately resolve the target resistivity also allows for improved estimates of hydrocarbon saturation from CSEM data.

The use of seismic velocity gradients to form the regularization weights for the CSEM inversion is just one example of a more general technique. Regularization weights could also be derived from any high-resolution data set that is a priori assumed to be structurally correlated with the CSEM resistivity. Although we have concentrated primarily on seismic full-waveform inversion models due to their high fidelity, nearby well logs and other data sets could also be used. Our test examples included correlated and uncorrelated seismic and electrical structure and showed the method to work best when the structures are correlated with large contrasts in velocity and resistivity. We also find that the method is relatively insensitive to depth errors of 100–200 m in the seismic velocity model, with the resulting seismically regularized CSEM inversion still recovering peak resistivities close to the true value. This approach was shown to perform poorly when the seismic and resistivity structures are strongly uncorrelated, but in such instances, the offset depths between the resistivity and seismic structures will verify that correlated structure required for seismically regularized inversion is not present.

There are limitations to the extent of any improvement in CSEM inversion models from using seismic regularization. For example, because CSEM data are not sensitive to very fine-scale layering, it is unlikely that seismic regularization will improve the resolution of such structures. Additionally, thin multiple stacked reservoir layers or very heterogeneous models with equivalent EM responses will be difficult to resolve due to nonuniqueness, even if the boundaries are well characterized by seismic velocity gradients. Although we have limited our tests to 1D models, we find no reason the method could not be applied to 2D and 3D modeling when resistivity and velocity are expected to be correlated.

ACKNOWLEDGMENTS

This work was supported by the Seafloor Electromagnetic Methods Consortium at Scripps Institution of Oceanography, the Lithos Consortium at University of Cambridge, and Institut de Physique du Globe de Paris. Three anonymous reviewers are thanked for their helpful comments.

REFERENCES

Bahr, D., E. Hutton, J. Syvitski, and L. Pratson, 2001, Exponential approximations to compacted sediment porosity profiles: Computers & Geosciences, **27**, 691–700, doi: 10.1016/S0098-3004(00)00140-0.

Carcione, J., B. Ursin, and J. Nordskag, 2007, Cross-property relations between electrical conductivity and the seismic velocity of rocks: Geophysics, **72**, no. 5, E193–E204, doi: 10.1190/1.2762224.

Constable, S., 2010, Ten years of marine CSEM for hydrocarbon exploration: Geophysics, **75**, no. 5, 75A67–75A81, doi: 10.1190/1.3483451.

Constable, S., , R. Parker, and C. Constableet al., 1987, Occam's inversion: A practical algorithm for generating smooth models from electromagnetic sounding data: Geophysics, **52**, 289–300, doi: 10.1190/1.1442303.

Constable, S., and C. J. Weiss, 2006, Mapping thin resistors and hydrocarbons with marine EM methods: Insights from 1D modeling: Geophysics, **71**, no. 2, G43–G51, doi: 10.1190/1.2187748.

Eidesmo, T., S. Ellingsrud, L. MacGregor, S. Constable, M. Sinha, S. Johansen, F. Kong, and H. Westerdahl, 2002, Sea bed logging (SBL), a new method for remote and direct identification of hydrocarbon filled layers in deepwater areas: First Break, **20**, 144–152.

Gallardo, L., and M. Meju, 2003, Characterization of heterogeneous near-surface materials by joint 2D inversion of DC resistivity and seismic data: Geophysical Research Letters, **30**, 1658, doi: 10.1029/2003GL017370.

Key, K., 2009, 1D inversion of multicomponent, multifrequency marine CSEM data: Methodology and synthetic studies for resolving thin resistive layers: Geophysics, **74**, no. 2, F9–F20, doi: 10.1190/1.3058434.

Key, K., and A. Lockwood, 2010, Determining the orientation of marine CSEM receivers using orthogonal procrustes rotation analysis: Geophysics, **75**, no. 3, F63–F70, doi: 10.1190/1.3378765.

Myer, D., S. Constable, and K. Key, 2011, Broad-band waveforms and robust processing for marine CSEM surveys: Geophysical Journal International, **184**, 689–698, doi: 10.1111/gji.2011.184.issue-2.

Neves, F., and S. Singh, 1996, Sensitivity study of seismic reflection/refraction data: Geophysical Journal International, **126**, 470–476, doi: 10.1111/gji.1996.126.issue-2.

Portniaguine, O., and M. Zhdanov, 1999, Focusing geophysical inversion images: Geophysics, **64**, 874–887, doi: 10.1190/1.1444596.

Shipp, R., E. Di Nicola-Carena, and S. Singh, 2005, 2D full wavefield inversion of wide angle real marine seismic data, 69th Annual International Meeting, SEG, Expanded Abstracts, 1394–1397.

Shipp, R., and S. Singh, 2002, Two-dimensional full wavefield inversion of wide-aperture marine seismic streamer data: Geophysical Journal International, **151**, 325–344, doi: 10.1046/j.1365-246X.2002.01645.x.

Tarantola, A., 1986, A strategy for nonlinear elastic inversion of seismic reflection data: Geophysics, **51**, 1893–1903, doi: 10.1190/1.1442046.

Tikhonov, A. N., and V. Y. Arsenin, 1977, Solutions of ill-posed problems: John Wiley & Sons Inc.

Virieux, J., and S. Operto, 2009, An overview of full-waveform inversion in exploration geophysics: Geophysics, **74**, no. 6, WCC1–WCC26, doi: 10.1190/1.3238367.